Near-Field Mapping of Plasmonic Antennas by Multiphoton Absorption in PMMA

Giorgio Volpe[†], *Monika Noack*[†§], *Srdjan S. Aćimović*[†], *Carsten Reinhardt*[§], *Romain Quidant*[*†‡]

[†] ICFO – Institut de Ciencies Fotoniques, Mediterranean Technology Park, 08860 Castelldefels (Barcelona), Spain

[§] Laser Zentrum Hannover e.V., Hollerithallee 8, D-30419 Hannover, Germany

[‡] ICREA – Istitució Catalana de Recerca i Estudis Avançats, 08010 Barcelona, Spain

* Corresponding author: romain.quidant@icfo.es

ABSTRACT

Mapping the optical near-field response around nanoantennas is a challenging, yet indispensable task in order to engineer light-matter interaction at the nanometer scale. Recently, photosensitive molecular probes, which undergo morphological or chemical changes induced by the local optical response of the nanostructures, have been proposed as a handy alternative to more cumbersome optical and electron-based techniques. Here, we report four-photon absorption in polymethyl-methacrylate (PMMA) as a very promising tool for nanoimaging the optical near-field around nanostructures over a broad range of near-infrared optical wavelengths. The high performance of our approach is demonstrated on single-rod antennas and coupled gap antennas

by comparing experimental maps with 3D numerical simulations of the electric near-field intensity.

KEYWORDS. Near-Field Mapping, Nanoantennas, Plasmonics, Photosensitive Polymers, PMMA, Multiphoton Absorption.

MANUSCRIPT TEXT

Optical antennas can efficiently couple to free propagating light and focus it into sub-wavelength volumes.[1] They therefore represent an unprecedented tool to tailor many light-matter interactions at the nanoscale, such as photodetection, light emission, sensing, and spectroscopy.[1] In most of these applications, full control and optimization of such antennas require a detailed and quantitative knowledge of their near-field response at the single-antenna level. Far-field imaging methods can spatially resolve the near field distribution of resonant plasmonic antennas for example using two-photon luminescence microscopy, although their resolution is limited by diffraction.[2] Alternatively, more sophisticated techniques, including electron energy loss spectroscopy (EELS),[3,4] photoemission electron microscopy (PEEM),[5] cathodoluminescence spectroscopy (CLS),[6] and near-field optical microscopy (SNOM),[7-9] can break the spatial resolution limit of conventional optics. However, these methods typically rely on complex setups that often make near-field measurements a cumbersome task. In the particular case of SNOM, the presence of the tip may additionally alter the intrinsic response of the nanostructure under study.[10-11] To avoid the complexity of these techniques, the use of photosensitive molecular probes has lately been proposed as a handy tool to map the optical near field generated by metallic nanoparticles, with a high resolution that is given by the technique used to image the molecular probe, such as electron-beam microscopy (SEM) or atomic force microscopy

(AFM).[12-15] Dipolar field profiles around silver and gold nanoparticles, in particular, have been successfully mapped with resolutions better than ten nm,[12-14] but previous attempts with molecular probes, such as SU8, failed to spatially resolve the mode distribution for higher order resonances.[12,15]

In this Letter, we propose the use of four-photon absorption in polymethyl-methacrylate (PMMA) as a novel strategy to generate direct sub-wavelength snapshots of the optical near-field response of plasmonic nanostructures. Our approach is tested on gold nanorods and gap antennas with increasing length, and it enables us to map the finest details of successive antenna modes up to the 5λ/2 resonance. Although very simple and easy to implement, the presented approach offers mode mapping in nanoantennas with a level of details that is comparable to advanced optical or electron-based techniques.[3-9] Moreover, our approach works over a broad range of near infrared optical wavelengths: a desirable feature when working with plasmonic antennas.

As a first test structure to demonstrate the potential of our method, we consider a simple antenna geometry formed by a single gold nanorod with increasing length, whose optical behavior has been extensively characterized both theoretically[16-17] and experimentally.[4,7,9,18] Our structures were fabricated by standard *e*-beam lithography on an ITO-coated glass substrate. The sample consisted of rod arrays of varying lengths (80 nm to 1 μm), while the rod width and height were fixed at 60 and 40 nm, respectively. An 80-nm-thick PMMA layer (AR-P 671.04 / Allresist GmbH, Germany) was spin-coated over the substrate to act as photosensitive molecular probe of the near-field distribution around the nanostructures. While PMMA has a linear absorption peak centered at 213 nm (blue solid line in Figure 1(a)), the PMMA-embedded nanorods are resonant in the near-infrared from 700 nm to 1 μm, as measured by the extinction

spectroscopy (inset of Figure 1(a)). In order to compensate for this wavelength mismatch, we employ the absorption of multiple infrared photons from the near field of the nanostructures to provide the PMMA enough energy to induce long-chain scission. Dipping the sample in a standard developer used in *e*-beam lithography (MIBK:IPA 1:1 / Microchem Co.) then makes it possible to selectively remove the exposed areas (Supporting Information). The illumination was provided by a tunable pulsed Ti:sapph laser (~200 fs pulses, 700-1000 nm), whose beam was slightly focused on the sample with a 40X objective with 0.65 numerical aperture (NA) in order to expose several structures at the time (approximately 800 nm at FWHM). In a typical experiment, the polarization of the beam was aligned along the longitudinal axes of the rods, and an incident power between 1 and 100 μW was provided per antenna during 30 s. After development, the sample was characterized by electron-beam microscopy with a resolution in the order of 10 nm.

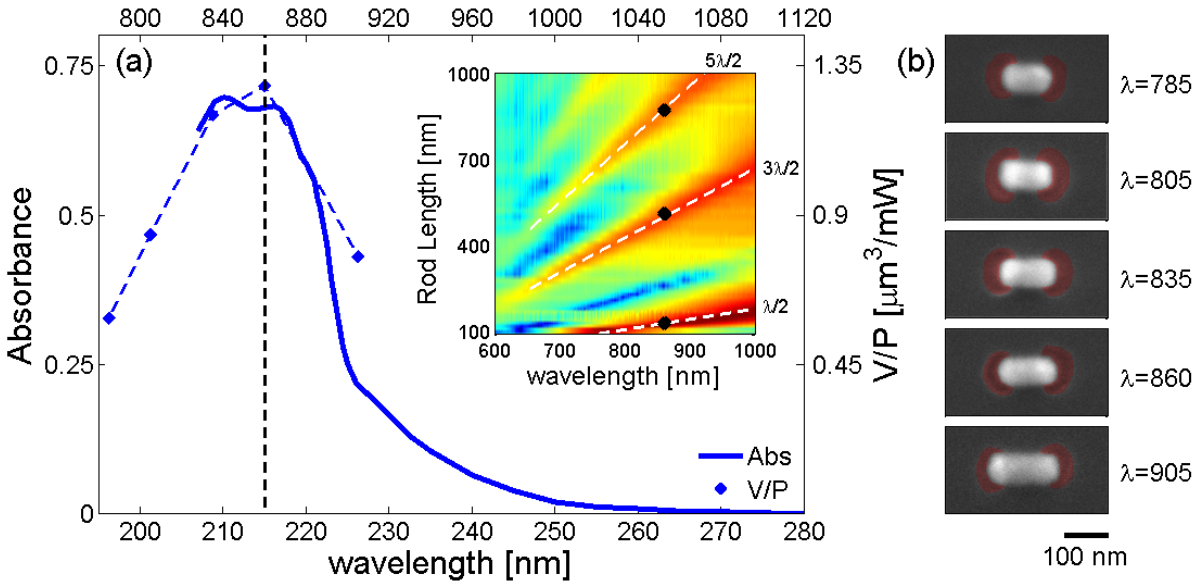

Figure 1. 4-photon PMMA absorption in the near field of gold nanorods. (a) Linear ultraviolet absorbance (blue solid line) of the PMMA used in the experiments (AR-P 671.04 / Allresist

GmbH, Germany), and average 4-photon-exposed volume in PMMA normalized to the incident power of light (blue dots) for five gold nanorod lengths with dipolar resonance at 785, 805, 835, 860 and 905 nm. The black dashed vertical line intersects the horizontal axes at 215 nm and 860 nm where the peak of the nonlinear curve lies. Inset: Evolution with the nanorods length of the measured extinction spectra (logarithmic scale). The white dashed lines highlight the evolution of the first three odd antenna modes ($\lambda/2$, $3\lambda/2$ and $5\lambda/2$), while the black dots point out the rod lengths resonant at 860 nm. (b) SEM images of exposed PMMA (highlighted in red) around five representative gold nanorods resonant at the wavelengths used to plot the nonlinear curve in (a). Scale bar: 100 nm.

The efficiency of the four-photon PMMA absorption as a function of the wavelength of light is monitored by the blue dots in Figure 1(a). These dots show a fixed range of exposed polymer volume normalized to the average power of the incident light for five nanorod lengths with dipolar resonances at 785, 805, 835, 860 and 905 nm, respectively. In terms of photon energies, the peak described by this curve overlaps well with the peak of the PMMA linear absorbance, and it has a maximum around 860 nm. This overlap enables us to conclude about the four-photon nature of this process: four photons at 860 nm indeed provide the same energy as one photon at 215 nm.

Figure 1(b) displays the SEM images of exposed PMMA around five representative gold nanorods resonant at the wavelengths used to plot the nonlinear curve in Figure 1(a). For contrast enhancement, an edge detection technique was adopted in order to highlight in red the exposed areas (Supporting Information). As other molecular probes before,[12-14] PMMA is able to effectively resolve the two lobes of highest field intensity at the rod ends, thus providing a

snapshot of the electric near-field intensity profile of the dipolar mode (λ/2). Furthermore, it has the advantage of working over a broad range of near-infrared wavelengths (broader than 100nm) where plasmonic localized resonances tend to lie.[2,4,18]

In reality, because of the four-photon nature of the absorption in PMMA, the exposure of the polymer around the nanostructures depends on the fourth power of the electric near-field intensity: above a certain power threshold and for a given exposure time, scission of the long chains in PMMA will occur until all the polymer chains within a certain volume are decross-linked, and with a rate that grows with the fourth power of the electric near-field intensity. This saturation process sets an upper limit to the sensitivity of the method within a certain volume. The exposed areas in Figure 1(b), therefore, represent a sample plane of the volume integral of the four-photon absorption process over the 80-nm-thick PMMA layer, thus recording the in-plane and out-of-plane evolution of the plasmonic mode within this volume. Moreover, the final recorded maps can also be affected by local changes of the polymer temperature or index of refraction due to the same exposure process. All these phenomena contribute to the definition of the exposed regions.

To get further insight on the performance of the method, Figure 2(a) shows the SEM images of exposed PMMA around the first three odd resonant modes (λ/2, 3λ/2 and 5λ/2) of a gold nanorods at 860 nm, the wavelength where the four-photon PMMA exposure shows the maximum efficiency in Figure 1(a): the lengths of these three nanorods (black dots in the inset of Figure 1(a)) are approximately 130, 515 and 880 nm. In general, plasmonic nanorods are resonant at lengths that are linearly related to integer multiples of half the wavelength λ_p of the surface wave propagating along the metal.[9,16-17] These integer numbers, which identify the order of the resonance, count the times the charge density changes sign along the antenna, while the

lobes that appear in the SEM images of Figure 2(a) are the points of highest charge density, where the electric near-field intensity is also maximum. As expected, in these images, two, four and six lobes can be clearly identified for the first-, third-, and fifth-order resonance, respectively. The distance between the centers of two consecutive lobes is half the plasmon wavelength λ_p, although, because of a non negligible phase shift upon reflection of the surface wave at the rod ends, λ_p can be more reliably determined from lobes at the center of the rods.[5,9] For example, a statistics over the distance between the centers of the two central lobes in the 3λ/2-antennas leads to λ_p = 349.37 ± 29.3 nm, which is in very good agreement with the value (λ_p = 347.08 ± 0.68 nm) that can be found when modeling the nanorod as a one-dimensional Fabry-Perót resonator.[9]

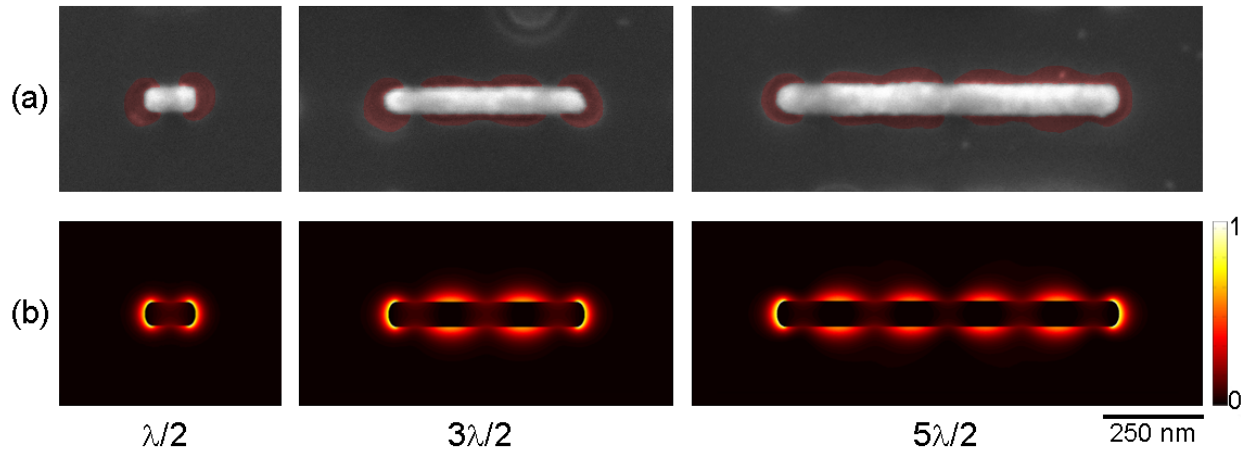

Figure 2. Mapping of successive odd resonant modes in gold nanorods with increasing lengths. (a) SEM images of exposed PMMA (highlighted in red) around a λ/2-, a 3λ/2- and a 5λ/2-antenna. All antennas are resonant at 860 nm (black dots in the inset of Figure 1(a)). For the three exposures, the incident power on the antennas is 4, 31 and 103 μW, respectively. (b)

Normalized electric near-field intensities computed in the half-plane of the rods in (a). Scale bar: 250 nm.

To further analyze our experimental data, Figure 2(b) shows the electric near-field intensities calculated in the half-plane of the previous nanorods using Comsol Multiphysics, commercial software based on finite element calculations (Supporting Information). In the calculations, the rods lie on a glass substrate and are embedded in an 80-nm-thick PMMA layer with a refractive index of 1.49. Despite the nonlinear nature and the complexity of the exposure process, by visual inspection, the experimental maps in PMMA reproduce well the spatial features of the calculated intensity distributions. The possibility of such a direct comparison makes possible to extract quantitative information about the plasmonic nanostructures, such as their plasmon wavelength, directly from the PMMA maps without having necessarily to develop post-processing tools of analysis to relate the modification in the topography of the molecular probe to the near-field intensity, as, for example, it is the case for the polarization-induced migration of azobenzene molecules.[12,19]

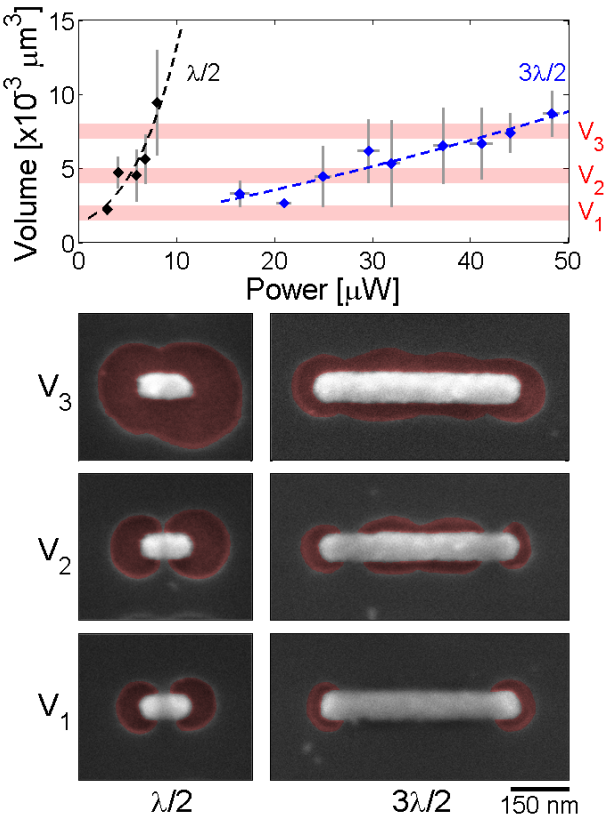

Figure 3. Power dependence of the exposed PMMA volume around gold nanorods. In the top graph, the black and blue dots (with the respective standard deviations in gray lines) represent the exposed volume in PMMA around λ/2- and 3λ/2-antennas resonant at 860 nm as a function of the incident power. The black and blue dashed lines fit the data with fourth-order power functions. The red areas highlight three increasing ranges of exposed volume V_1, V_2, and V_3, going from very confined exposures (V_1) to overexposures (V_3). At the bottom, representative SEM images of exposed PMMA (highlighted in red) for these different volume levels are shown both for the λ/2- and 3λ/2-antennas. Scale bar: 150 nm.

In a similar way to other molecular probes before, the power delivered to an antenna for a fixed illumination time is like a knob we can twist to tune the volume of the exposed polymer

around the nanostructure. To provide more quantitative information about the ranges of power needed for the near-field mapping of the antennas, the top graph in Figure 3 characterizes the average power dependence around λ/2-antennas (black dots) and 3λ/2-antennas (blue dots) with the same resonant lengths of those in Figure 2. Due to the difference in the enhancement factor between the two geometries, typical incident powers vary from approximately 3 to 10 μW for λ/2-antennas, and from approximately 15 to 50 μW for 3λ/2-antennas before any thermal contribution can be clearly observed in the exposed polymer, thus leading to homogeneous exposures around the nanorods,[15] according to the temperature gradient which decays with the inverse of the distance from the metal.[20] These levels of power are well below the damage threshold of the gold structures, as confirmed by a recent study on four-photon absorption in gold nanoantennas,[21] while much lower values do not expose the polymer to its surface so that no pattern can be developed. For every resonant order, the points in the graph are averaged over more than 60 different structures: as the large error bars (gray lines) attest, the original set of data is substantially scattered around the average points. This spreading is mostly attributed to the highly nonlinear nature of the process, thus making the exposure of the PMMA around the rods very sensitive to inter-rod variability and defects due to fabrication. The black and blue dashed lines fit the data to fourth-order power functions, whose great difference in slope also reflects the difference in enhancement between the two resonant orders. These functional dependences break down approximately above and below the typical incident powers reported above, when the developed maps reveal either thermal effects or no exposure at all, respectively. The red areas highlight three ranges of exposed volume V_1, V_2, and V_3, and they intersect the two data points over different ranges of incident power. At the bottom of Figure 3, typical SEM images of exposed PMMA for these volume levels are shown both for the λ/2- and 3λ/2-antennas. Going

from very confined exposures (V1) to overexposures (V3), these images monitor the different magnitude levels of the electric near-field around the nanorods as a function of the incident power. For the λ/2-antennas, the pattern imposed by the two lobes of maximum field intensity can always be recognized at increasing levels of exposed PMMA volume. For the 3λ/2-antennas, low incident powers only expose the rod ends, the points of strongest field enhancement.[2,16] At intermediate power levels, the lobes along the nanorod also appear, as already noticed in Figure 2(a). Eventually, at higher powers, the PMMA around the antenna is completely exposed. As shown in a previous work for a different molecular probe,[13] the information about the extent of the exposure around the nanostructures as a function of the incident power or wavelength can be used to characterize the plasmonic modes in a more quantitative way.

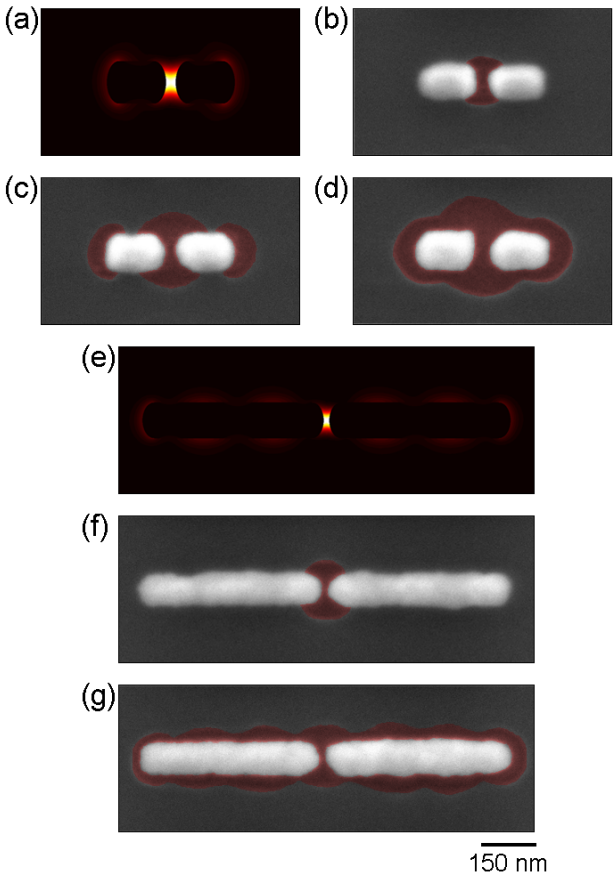

Figure 4. Mapping resonant modes in plasmonic gap antennas. Normalized electric near-field intensities computed in the half-plane of the first-order (a) and third-order (e) resonant mode of gap antennas resonant at 860 nm. (b-d) SEM images of exposed PMMA (highlighted in red) around the first-order resonance for three increasing levels of exposed polymer volume. (f-g) Equivalent SEM images around the third-order resonance for two levels of exposed volume. Scale bar: 150 nm.

In what follows, we show the applicability of the imaging method based on the four-photon absorption in PMMA to more complex plasmonic geometries. We focus on the case of a gap antenna, whose optical behavior is also very well characterized in the literature.[2,16] Extinction measurements were performed to identify the structures with first-order and third-order resonance at 860 nm (data not shown). Illumination and exposure conditions similar to the nanorod case were used. In particular, the polarization of the beam was aligned along the longitudinal axes of the antenna arms in order to excite the antenna bonding mode.[17] Figure 4(a) and (e) show the expected electric near-field intensities computed in the half-plane for the two identified resonant geometries. Figure 4(b-d) show SEM images of exposed PMMA around the first-order resonant geometry for three volume levels of exposed PMMA, while Figure 4(f-g) show equivalent SEM images around the third-order resonant geometry. As previously noted for the single nanorods, despite the complexity of the exposure process, a good agreement between the location of the spatial features of the calculated and experimental maps is found also for the gap antenna case: going from very confined exposures to overexposures, the experimental maps are able to monitor the different magnitude levels of the electric near-field around the nanostructures. In Figure 4(b) and (f), for low volume levels of exposed PMMA, only the gap is

visible, since it is the point of strongest field enhancement.[2,16] For higher values of exposed volumes in Figure 4(c) and (g), we can also observe the lobes at the extreme of and, for the third-order resonant geometry, within the arms of the gap antennas, where the highest charge density resides within the structures. Finally, Figure 4(d) shows a case of overexposure for the first-order resonant geometry.

In conclusion, we have introduced and tested a novel technique to map the electric near-field distribution around nanostructures based on four-photon absorption in PMMA, a widespread lithographic resist, with unprecedented spatial detail for a molecular probe. We characterized the performance of the method by mapping the localized electric near-field generated by two emblematic antenna geometries, a rod and a gap nanoantenna. The obtained maps monitor the spatial evolution of the electric near-field intensity around the antennas, and directly relate to the calculated electric near-field intensity distribution around the nanostructures. The introduction of an asymmetry in the illumination, such as a tilt or a spatially shaped wavefront, could allow one to readily map also the dark plasmonic modes around such or more complex nanostructures.[22,23] Moreover, the method leaves room for improvement: factors, such as the PMMA molecular weight, its thickness or the temperature at which the experiments are performed, could substantially improve the final resolution of the generated maps. This straightforward method can complement well already existing and more established techniques, such as SNOM and PEEM. In particular, optical antenna designs could definitely benefit from the possibility of visualizing complex local plasmonic responses, such as plasmonic dark modes, in an easy and fast way.

ASSOCIATED CONTENT

Supporting Information. Additional parameters for the exposure and development of the PMMA, details on the numerical calculations with COMSOL Multiphysics, and edge detection technique used to process the SEM images. This material is available free of charge via the Internet at http://pubs.acs.org.

AUTHOR INFORMATION

Author Contributions

S.S.A., G.V. and R.Q. conceived the experiment; G.V. and S.S.A fabricated the samples; G.V. and M.N. developed the method, performed the experiments, and analyzed the data; S.S.A performed the FEM simulations; G.V. wrote the manuscript; C.R. and R.Q supervised the project. All authors discussed the results and commented on the final manuscript.

ACKNOWLEDGMENT

This work was supported by ERC-2010-StG Plasmolight (Grant No: 259196), and Fundació Privada CELLEX. Additionally, M.N. and C.R. acknowledge financial support by the Centre for Quantum Engineering and Space-Time Research (QUEST). C.R. further acknowledges the priority program SPP1391 "Ultrafast Nanooptics" of the Deutsche Forschungsgemeinschaft (DFG). We thank Jan Renger and Mark P. Kreuzer for fruitful discussions.

REFERENCES

(1) Novotny, L.; van Hulst, N. F. *Nat. Photonics* **2011**, *5*, 83-90.

(2) Ghenuche, P.; Cherukulappurath, S.; Taminiau, T. H.; van Hulst, N. F.; Quidant, R. *Phys. Rev. Lett.* **2008**, *101*, 116805.

(3) Nelayah, J.; Kociak, M.; Stéphan, O.; García de Abajo, F. J.; Tencé, M.; Henrard, L.; Taverna, D.; Pastoriza-Santos, I.; Liz-Marzán, L. M.; Colliex, C. *Nat. Phys.* **2007**, *3*, 348–353.

(4) Bosman, M.; Keast, V. J.; Watanabe, M.; Maaroof, A. I.; Cortie, M. B. *Nanotechnology* **2007**, *18*, 165505.

(5) Vesseur, E. J. R.; de Waele, R.; Kuttge, M.; Polman, A. *Nano Lett*. **2007**, *7*, 2843-2846.

(6) Douillard, L.; Charra, F.; Korczak, Z.; Bachelot, R.; Kostcheev, S.; Lerondel, G.; Adam, P. M.; Royer, P. *Nano Lett.* **2008**, *8*, 935–940.

(7) Imura, K.; Nagahara, T.; Okamoto, H. *J. Am. Chem. Soc*. **2004**, *126*, 12730-12731.

(8) Esteban, R.; Vogelgesang, R.; Dorfmüller, J.; Dmitriev, A.; Rockstuhl, C.; Etrich, C.; Kern, K. *Nano Lett.* **2008**, *8*, 3155–3159.

(9) Dorfmüller, J.; Vogelgesang, R.; Weitz, R. T.; Rockstuhl, C.; Etrich, C.; Pertsch, T.; Lederer, F.; Kern, K. *Nano Lett.* **2009**, *9*, 2372–2377.

(10) Lereu, A. L.; Sanchez-Mosteiro, G.; Ghenuche, P.; Quidant, R.; van Hulst, N. F. *J. Microsc*. **2008**, *229*, 254-258.

(11) García-Etxarri, A.; Romero, I.; García de Abajo, F. J.; Hillenbrand, R.; Aizpurua, J. *Phys. Rev. B* **2009**, *79*, 125439.

(12) Hubert, C.; Rumyantseva, A.; Lerondel, G.; Grand, J.; Kostcheev, S.; Billot, L.; Vial, A.; Bachelot, R.; Royer, P.; Chang, S. H.; Gray, S. K.; Wiederrecht, G. P.; Schatz, G. C. *Nano Lett*. **2005**, *5*, 615-619.

(13) Deeb, C.; Bachelot, R.; Plain, J.; Baudrion, A. L.; Jradi, S.; Bouhelier, A.; Soppera, O.; Jain, P. K.; Huang, L.; Ecoffet, C.; Balan, L.; Royer, P. *ACS Nano* **2010**, *4*, 4579-4586.

(14) Ueno, K.; Juodkazis, S.; Shibuya, T.; Yokota, Y.; Mizeikis, V.; Sasaki, K.; Misawa, H. *J. Am. Chem. Soc.* **2008**, *130*, 6928-6929.

(15) Murazawa, N.; Ueno, K.; Mizeikis, V.; Juodkazis, S.; Misawa, H. *J. Phys. Chem. C* **2009**, *113*, 1147-1149.

(16) Aizpurua, J.; Bryant, G. W.; Richter, L. J.; García de Abajo, F. J.; Kelley, B. K.; Mallouk, T. *Phys. Rev. B* **2005**, *71*, 235420.

(17) Novotny, L. *Phys. Rev. Lett.* **2007**, *98*, 266802.

(18) Schider, G.; Krenn, J. R.; Hohenau, A.; Ditlbacher, H.; Leitner, A.; Aussenegg, F. R.; Schaich, W. L.; Puscasu, I.; Monacelli, B.; Boreman, G. *Phys. Rev. B* **2003**, *68*, 155427.

(19) Juan, M. L.; Plain, J.; Bachelot, R.; Royer, P.; Gray, S. K.; Wiederrecht, G. P. *ACS Nano* **2009**, *6*, 1573-1579.

(20) Baffou, G.; Quidant, R. *Laser Photonics Rev.* **2012**, DOI: 10.1002/lpor.201200003.

(21) Biagioni, P.; Brida, D.; Huang, J. S.; Kern, J.; Duò, L.; Hecht, B.; Finazzi M.; Cerullo G. *Nano Lett.* **2012**, DOI: 10.1021/nl300616s.

(22) Volpe, G.; Cherukulappurath, S.; Juanola Parramon, R.; Molina-Terriza, G.; Quidant R. *Nano Lett.* **2009**, *9*, 3608-3611.

(23) Huang, J. S.; Kern, J.; Geisler, P.; Weinmann, P.; Kamp, M.; Forchel, A.; Biagioni, P.; Hecht, B. *Nano Lett.* **2010**, *10*, 2105-2110.